arXiv:1612.06199v1 [cond-mat.mes-hall] 19 Dec 2016

Anisotropy and suppression of spin-flip tunneling

A. Hofmann,* V. F. Maisi, T. Krähenmann, C. Reichl, W. Wegscheider, K. Ensslin, and T. Ihn
Laboratory for Solid State Physics, ETH Zurich, 8093 Zurich, Switzerland

(Dated: December 20, 2016)

We measure the spin-flip tunneling rates in GaAs-based double quantum dots by time-resolved charge detection of two electrons in the Pauli spin blockade regime. With the orientation of the double quantum dot device, we are able to select the direction of the electron momentum with respect to the crystallographic axes of the sample, and thereby the amplitude and direction of the spin-orbit field experienced by the tunnrlin electron. The dependence of the spin-flip tunneling rate on the tunnel-coupling is sensitive to the strength of the spin-orbit interaction in the chosen direction. We find different strengths depending on the crystallographic orientation of the double quantum dot, which is a consequence of the anisotropy of the spin-orbit interaction. With a given orientation, we further measure the anisotropy of the spin-flip tunneling rate induced by rotating the external in-plane magnetic field, thereby changing the angle between the spin quantization axis and the perturbing spin-orbit field. We find a suppressed spin-flip tunneling rate for electrons tunneling along the [$\bar{1}$10] crystallographic direction compared to the [110] direction, indicating that $\alpha \approx \beta$.For high magnetic fields, we measure resonant spin-flip tunnelling, which we can suppress almost completely by orienting the in-plane field perpendicular to the spin-orbit field.

Electron spin qubits undergo decoherence by coupling to nuclear spins and to the orbital motion in the crystal [1]. In our experiments we suppress the first mechanism by applying a sufficient external magnetic field larger than the hyperfine Overhauser field. This allows us to investigate spin-orbit-coupling related spin-flip processes. In double dot systems, spin flips occur both within a dot [2] and during tunneling between the dots [3]. The intra-dot process depends on the geometry of the dot and its orientation with respect to the crystal lattice [4–10].

Here we show experimentally that flipping an electronic spin by spin-orbit interaction during tunneling can be controlled and almost completely suppressed by orienting a double dot system with respect to external magnetic field and crystal lattice. The orientation of the double quantum dot axis, which defines the direction of inter-dot tunneling, selects magnitude and direction of the spin-orbit field relevant for spin-flip tunneling. For disticnt orientations, we extract the different magnitudes from the dependence of the spin-flip tunneling rate on the inter-dot tunnel-coupling following theoretical work by J. Danon [9]. We find a suppressed spin-orbit interaction in [$\bar{1}$10]-direction compared to the [110]-direction. For a given orientation, we further measure the anisotropy of the spin-flip tunneling rate brought about by the orientation of the external magnetic field with respect to the crystal lattice. The latter changes the angle between the spin quantization axis within the dots and the spin-orbit field relevant during tunneling [11]. For a large enough magnetic field, the spin-flip tunneling can be completely suppressed within measurement accuracy. The toolbox comprising single-dot orientation, tunneling direction, and external magnetic field enables tuning and controlling spin relaxation caused by spin-orbit interaction for spin qubits in semiconductor double dots.

The GaAs/AlGaAs heterostructure used here contains a two-dimensional electron gas 90 nm below the surface

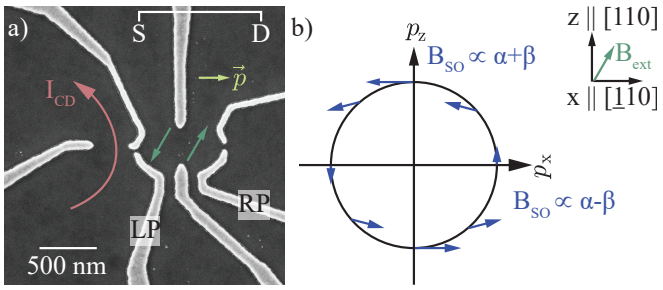

FIG. 1. Sample layout. (a) A scanning electron micrograph of one part of the sample, showing top-gates in light grey and parts of the two-dimensional electron gas in dark grey color. The current I_{CD} measures the charge state of the two electrons (green arrows) occupying the double quantum dot. Source (S) and drain (D) contacts are connected to remain on the same potential. The direction of the electron momentum is given by the main axis of the DQD and is indicated by $\vec{p}$. (b) shows the spin-orbit magnetic field experienced by an electron in our structure with momentum $\vec{p}$ [9]. In the two directions [110] or [$\bar{1}$10] the Rashba (α) and Dresselhaus (β) contributions either add up or cancel each other, respectively. The picture shows the case where $\alpha \approx \beta$.

with an electron density $n = 2 \times 10^{11}\,\mathrm{cm}^{-2}$ and mobility $\mu = 2 \times 10^{6}\,\mathrm{cm}^2/\mathrm{Vs}$ as measured at 1.3 K. We pattern metallic (Ti/Au) gates on top of the heterostructure in order to form two separate double quantum dots (DQDs), one of which is shown in Fig. 1(a). Negative voltages applied to top gates (light-grey fingers) deplete the two-dimensional electron gas (dark-grey area) and confine the electrons (green arrows) in the double quantum dot [1]. The same gate design is patterned twice onto a single chip, separated by 40 μm. The principal axis of tunneling between the two dots forming the DQD is indicated with the momentum $\vec{p}$ (yellow) in Fig. 1(a) and points along the [110] crystal axis for DQD1 and along [$\bar{1}$10] for

DQD2. The results shown in this paper are obtained by measuring the two devices on the same chip. The base temperature of the cryostat is 10 mK and the temperature of the two-dimensional electron gas is $T = 50$ mK as measured by Coulomb blockade thermometry [12, 13]. In-plane magnetic fields can be applied at arbitrary angles using a vector magnet.

For each double quantum dot, the voltages on the gates LP and RP shift the energies of the quantum states in the left and right dot, respectively, and move all quantum states above the Fermi energy of the source and drain reservoirs, such that no electron remains in the DQD. The number $N_{\mathrm{L,R}}$ of electrons in the right and left dot is indicated as paris (N_L, N_R) in the following. Our measurements are performed at a gate voltage configuration where the charge states $(0, 2)$ and $(1, 1)$ are degenerate. The DQD is isolated from the reservoirs by Coulomb blockade and a small tunnel coupling, such that the resulting tunneling rates to source and drain are expected to be below 0.01 Hz. Two electrons reside in the DQD in a way that the right dot always contains at least one electron, and one electron tunnels back and forth between the left and right quantum dot.

These tunneling events are observed in real time by measuring the current I_{CD} through the constriction close to the device [see Fig. 1(a)] [14, 15]. The current through the constriction is sensitive to changes in its electrostatic environment. Thus, the current changes between two values depending on whether the excess electron resides on the left or the right quantum dot. In Fig. 2(a), the current is higher, if the electron is in the right quantum dot, hence the charge state is $(0, 2)$, and lower if it occupies the left quantum dot, hence the two electrons occupy different quantum dots [charge state $(1, 1)$].

From time traces like those shown in Fig. 2(a), we directly read the waiting times $\tau_{R/L}$ for the electron to reside in the right/left quantum dot. A histogram of these waiting times shows the exponential decay of the $(0, 2)$ state, with the decay rate determined by the tunneling rate Γ_{C}, as shown in the inset of Fig. 2(b) with green squares [3]. The rate Γ_{C} is a spin-conserving tunneling rate of one electron from the right to the left quantum dot and is a measure for the tunnel-coupling between the two dots, which is set to the order of 100 Hz (tunnel-coupling of the order neV) in our experiment. At small external magnetic field, $|B| \geq 30$ mT, the decay of the $(1, 1)$ state (tunneling of an electron from the left to the right dot) is governed by two different time scales. This is a consequence of the Pauli spin blockade effect in a double-quantum dot occupied by an even number of electrons [3, 16–19], as described in the following.

The $(0, 2)$ charge state is a singlet state, with two antiparallel electron spins. [20]. At zero magnetic field and small tunnel coupling, the $(1, 1)$ charge state is fourfold degenerate with two almost independent electron spins. We therefore choose as a basis for the $(1, 1)$ charge state the four spin states $\{|\uparrow\uparrow\rangle, |\uparrow\downarrow\rangle, |\downarrow\uparrow\rangle, |\downarrow\downarrow\rangle\}$, where the two arrows indicate the orientation of the electron spin in the left and right quantum dot with respect to the respective quantization axis. [1, 3]. The Overhauser fields in the two dots are of the order of a few mT [21] with a random and uncorrelated orientation and define the respective spin quantization axis in these dots. The hyperfine interaction thereby mixes the four $(1, 1)$ spin states on the time-scale of nanoseconds.

With an external magnetic field larger than the Overhauser fields, the spin quantization axis in both dots is the same and given by the direction of the external magnetic field. The four $(1, 1)$ spin states are occupied with equal probability (thermodynamic equipartition [22]) as long as the Zeeman splitting is much smaller than the thermal energy. However, mixing of the spin-polarized with the non-polarized states is suppressed [23]. This slow mixing changes the tunneling dynamics. Electrons tunnel from the unpolarized $(1, 1)$ state into the $(0, 2)$ state at a rate $\Gamma_C/2$ [3], determined only by the tunnel-coupling between the two dots. However, a spin-flip is required for the tunneling from the polarized state [3, 18], and needs to be mediated by spin-orbit or hyperfine interaction. This gives rise to the long waiting times in the $(1, 1)$ state in Fig. 2(a) and the long time-scale in Fig. 2(b), which we identify with the spin-flip rate Γ_{S}. The waiting time distributions of back-and-forth tunneling between the left and right quantum dot as shown in Fig. 2 hence provides the spin-conserving tunneling rate Γ_{C} as well as the spin-flip rate Γ_{S}.

The spin-flip rate Γ_{S} depends on the process which mediates mixing between the four $(1, 1)$ states. It is well-known that the dominating mechanisms for a spin-flip are the hyperfine interaction and the spin-orbit interaction. The spin-orbit interaction induces spin-flips in two ways. First, the spin-orbit interaction is present in each of the single quantum dots, and leads to quantum mechanical mixing of the four $(1, 1)$ charge states [2, 4, 5]. This spin-flip mechanism, together with the hyperfine interaction both describe spin flips within a single dot, and lead to a spin-flip rate which we denote with Γ_{int}.

A second mechanism leading to spin-flips is the spin-orbit interaction which arises only due to the finite coupling between two dots. In a classical picture, an electron moves from one dot to another and feels a magnetic field, the spin-orbit field, due to the electric field arising from the structure (Rashba effect) and bulk (Dresselhaus effect) inversion asymmetries. If the spin-orbit field has a component perpendicular to the electron magnetic moment, it precesses about this field, leading to a spin-flip. The size and orientation of the spin-orbit field depends on the direction of the electron momentum with respect to the crystallographic axes, as shown in Fig. 1(b), where we plot the spin-orbit field vector experienced by moving electron in blue for different orientations of its momentum. In our double quantum dot device, the momentum

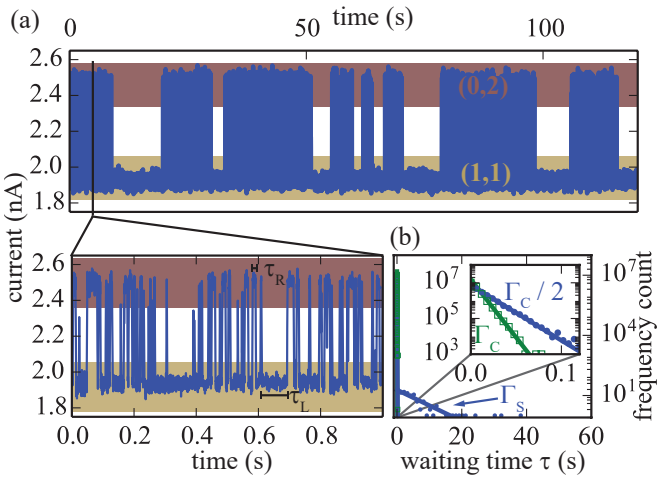

FIG. 2. Charge detection. (a) The charge detector current I_{CD} changes between two values, depending on the charge state of the two-electron DQD. The bunching of tunneling events is visible in the long time trace, and the zoom shows the fast tunneling events when the electron spins are antiparallel. The waiting time distribution is plotted in (b), where green and blue symbols are used for the decay of the $(0,2)$ and $(1,1)$ state, respectively. The slow time-scale (spin-flip rate) is visible in the main figure and the fast time-scale (spin-conserving rates) in the inset, which is a zoom of the main figure.

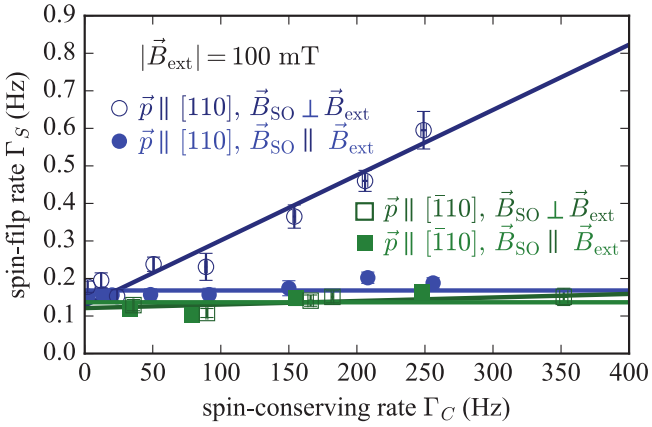

FIG. 3. The spin-flip rate as a function of the spin-conserving rate at an externally applied magnetic field of 100 mT. The blue circles represent data taken from DQD1 ($\vec{p} \parallel [110]$) and green squares are used for DQD2 ($\vec{p} \parallel [\bar{1}10]$). Open symbols are used for perpendicular alignment of the spin quantization axis and the perturbing spin-orbit field, and filled symbols for the parallel alignment. The suppression of the spin-orbit interaction is visible in the vanishing dependence of the spin-flip rate on the tunnel coupling.

$\vec{p}$ is determined by the orientation of the device with respect to the crystallographic axes and is chosen by lithography. In this configuration, we expect $\vec{B}_{\mathrm{SO}} \parallel [\bar{1}10]$ for DQD1, and $\vec{B}_{\mathrm{SO}} \parallel [110]$ for DQD2, independent of the relative size and sign of the spin-orbit coupling constants, α and β. This kind of spin-orbit interaction leads to a spin-flip tunneling rate, here called Γ_{SO}, which depends on the tunnel coupling between the two coupled quantum dots.

In the experiment, we observe that the spin-flip rate Γ_{S}, which we extract from the slow time-scale of the waiting time distributions [cf Fig. 2(b)], depends linearly on the tunneling rate Γ_{C}, with a finite offset. The linear dependence is shown in Fig. 3 for DQD1 with blue circles and for DQD2 with green squares. The open and closed symbols represent different alignments of the external magnetic field B_{ext} with respect to the expected spin-orbit field B_{SO}. With the above considerations, we identify the contribution to Γ_{S} which is dependent on the tunnel-coupling with the spin-flip tunneling rate Γ_{SO}. We argue that the remaining spin-flip rate at zero tunnel coupling arises from internal relaxation processes Γ_{int} within a single dot, which are independent of the tunnel-coupling [3, 9]. This gives

$$\Gamma_{\mathrm{S}} = \Gamma_{\mathrm{int}} + \Gamma_{\mathrm{SO}} \tag{1}$$

Even though the classical picture given above is not fully accurate [24], it is in accordance with the spin-flip tunneling rate which has been calculated for example in Ref. 9, Eqs. (6, 9), utilizing quantum theory. There, the spin-orbit Hamiltonian, H_{SO}, couples the $(0,2)$ state to the polarized $(1,1)$ states, which leads to a spin-flip tunneling rate:

$$H_{\mathrm{SO}} = \alpha[p_z\sigma_x - p_x\sigma_z] + \beta[p_x\sigma_z + p_z\sigma_x] \tag{2a}$$

$$\Gamma_{\mathrm{SO}} = \frac{d^2}{2l_{\mathrm{SO}}^2}\Gamma_{\mathrm{C}}\sin^2(\phi), \phi = \measuredangle(\vec{B}_{SO}, \vec{B}_{\mathrm{ext}}) \tag{2b}$$

The coordinate system is defined in the plane of a GaAs heterostructure grown along [001] direction, with $x \parallel [\bar{1}10]$ and $z \parallel [110]$, as indicated in Fig 1, and σ_i are the Pauli matrices. The spin-flip tunneling rate is proportional to the ratio of the inter-dot distance d (classical: the distance over which the electron spin can precess) and the spin-orbit length l_{SO} (classical: the length required for the spin to rotate by 2π). The spin-orbit length is different for the two devices, $l_{\mathrm{SO}} = \hbar/m^*(\alpha \pm \beta)$, with the plus or minus sign valid for the tunneling direction in DQD1 or DQD2, respectively. The Rashba (α) and Dresselhaus (β) spin-orbit coefficients are unknown a-priori, and $m^* = 0.067m_e$ is the electron mass in GaAs. The spin-orbit field does not cause a spin-flip tunneling rate if the spin-orbit field is parallel to the external magnetic field ($\phi = 0$).

Following Eqs. (1) and (2b), we measure Γ_{S} and find the strength of the relevant spin-orbit interaction from its contribution linear in Γ_{C}. In a first step, we fix $\phi = 90°$ - in the experiment, this means that the external field is along z in DQD1 or along x in DQD2 - and measure $\Gamma_{\mathrm{SO}}/\Gamma_{\mathrm{C}}$ from the slope in Fig. 3. We find a larger slope

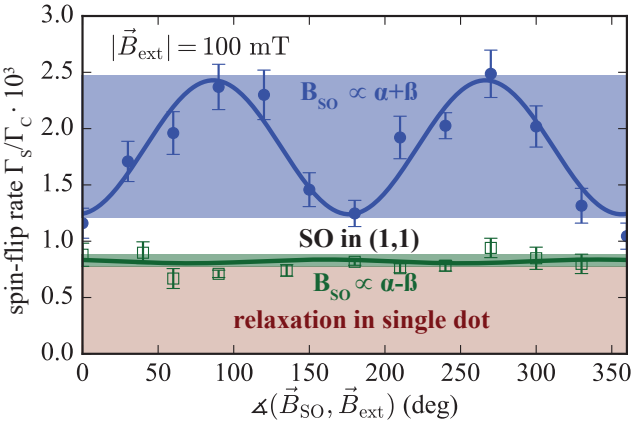
$|\vec{B}_{\rm ext}| = 100$ mT
$B_{SO} \propto \alpha+\beta$
SO in (1,1)
$B_{SO} \propto \alpha-\beta$
relaxation in single dot
spin-flip rate $\Gamma_s/\Gamma_C \cdot 10^3$
$\measuredangle(\vec{B}_{\rm SO}, \vec{B}_{\rm ext})$ (deg)

FIG. 4. The spin-flip rate normalized to the spin-conserving rate as a function of the in-plane angle ϕ between the external field (spin quantization axis) and the spin-orbit field (perturbation). The sinusoidal dependence found in DQD2 (filled blue circles) reflects the anisotropy of the perturbation induced by the spin-orbit interaction. The spin-orbit interaction vanishes for DQD1 (open green squares), leading to an almost isotropic spin-flip rate. The isotropic background is determined by the spin-flip processes within the $(1,1)$ charge state in the individual DQD devices.

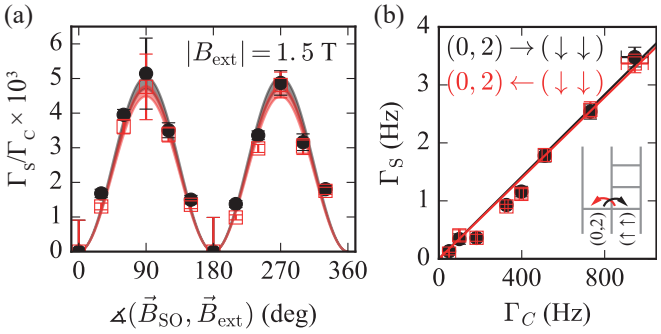

FIG. 5. Spin-flip tunneling rate at a magnetic field of 1.5 T for the device DQD1. Black and red data points denote the decay of the $(0,2)$ and $(\downarrow\downarrow)$ states, respectively. (a) shows the anisotropy of the spin-flip tunneling depending on the in-plane magnetic field direction. The solid line is a fit to Eq. (2b). The linear dependence of the spin-flip tunneling is plotted in (b). The solid line is a linear fit without an offset. The inset illustrates the two tunneling processes between the resonant ground states.

for DQD1 (blue closed circles) than for DQD2 (green open squares), meaning that $(\alpha+\beta) > (\alpha-\beta)$. In fact, the slope almost vanishes in DQD2, indicating that the two coefficients have a similar amplitude and the same sign, hence $\alpha - \beta \approx 0$. Comparing the two slopes, we determine an upper bound for the relative difference of the two spin-orbit parameters and find that the spin-orbit interaction for electrons moving along $[\bar{1}10]$ is suppressed by a factor $\left|\frac{\alpha-\beta}{\alpha+\beta}\right|^2 \leq 5\times10^{-2}$ compared to the $[110]$ direction. With a distance $d \approx 300\,$nm between the two quantum dots, we estimate $\alpha \approx \beta \approx 1.5\times10^3\,\mathrm{m\,s^{-1}}$, which agrees well with spin-orbit lengths of few μm found in literature [3, 11, 25]. Second, we fix $\phi = 0°$ and find that the slopes are vanishingly small in both DQD devices [open symbols in Fig. 3] indicating negligible spin-flip tunneling $\Gamma_{\rm SO}$. This agrees with the theoretical expectation in Eqs. (2) as well as with our classical interpretation that the absence of a perpendicular component prevents the precession of the magnetic moment in the spin-orbit field, independent of its amplitude.

To further study the anisotropy of the spin-flip rate, we fix the tunneling coupling constant $\Gamma_C = 160$ Hz and vary ϕ by rotating the in-plane direction of the magnetic field. The results are shown in Fig. 4 with the blue filled circles for the electron momentum along z (DQD1) and green open squares for the momentum along x (DQD2). We find a sinusoidal dependence on ϕ for the spin-flip rate measured in DQD1, and almost isotropic relaxation for DQD2, as expected from Eq. (2b). Consistent with the data presented in Fig. 3, the minima and maxima occur at $\phi = 0°, 180°$ and $\phi = 90°, 270°$, respectively. The solid lines are fits to $[\Gamma_{\rm int}/\Gamma_C + c_\pm \sin^2(\measuredangle(\phi+\phi_0))]$, as described in Eqs. (2) with $\Gamma_{\rm int}$, $c_\pm$ and ϕ_0 as fitting parameters. The phase offset ϕ_0 accounts for an uncertainty in the alignment of the sample with respect to the magnetic field, which we expect to be smaller than 5 degrees.

The internal relaxation [$\Gamma_{\rm int}$ in Eq. 2] adds an isotropic contribution to the spin-flip rate independent on the tunneling coupling. This contribution is similar in the two DQD devices, as evident, for example, from the offset to the sinusoidal data in Fig. 4, or the spin-flip rate at zero tunneling coupling in Fig. 3. While similar internal relaxation rates indicate a similar hyperfine spin environment in all four dots, slight variations can occur due to different internal spin-orbit coupling strength given by the individual electron wave-functions in each of the single quantum dots [2].

A large external field of $|B_{\rm ext}| = 1.5$ T allows us to suppress the internal relaxation and study the bare spin-flip tunnelling: Due to the large Zeeman-splitting, the $|\downarrow\downarrow\rangle$ is the ground state, and excitations to the unpolarized states are suppressed. In order to measure and tune Γ_C (the tunneling rate between the $(0,2)$ and the unpolarized states) we utilize a feedback mechanism [26], which initializes the device in the $(0,2)$ state and then drives this state in resonance with the unpolarized $(1,1)$ charge state. With the external field perpendicular to the spin-orbit field, $\phi = 90°$, we again find that the spin-flip rate is linear in Γ_C, as shown in Fig. 5(b). In contrast to the experiment at lower field, the spin-flip rate extrapolates to zero when the tunneling coupling is reduced, indicating the vanishing effect of internal relaxation processes. The black and red data points in Fig. 5 represent the tunneling rates in the two directions, $(0,2) \rightarrow |\downarrow\downarrow\rangle$ and $(0,2) \leftarrow |\downarrow\downarrow\rangle$, respectively. They are equal within error

bars, indicating that both levels have the same degeneracy (non-degenerate) [26]. This holds true if the excited states have a negligible effect to the tunneling process.

Having suppressed the internal relaxation, we measure the spin-flip tunnelling rate in the configuration of the double quantum dot shown in the inset if Fig. 5(b). The electrons spin-flip tunnel resonantely between the two dots, which means that the observed spin-flip tunneling can in principle be a coherent process. Varying the angle ϕ, as shown in Fig. 5(a), the spin-flip tunneling rate follows the sinusoidal curve expected from Eq. (2b), and is fully suppressed at the specific angles $\phi = 0°, 180°$, where the external field is parallel to the spin-orbit magnetic field.

In conclusion, we have demonstrated the selective measurement of the spin-orbit interaction strength for a chosen momentum vector of the electron. We have determined the contribution of the spin-orbit interaction to the spin-flip time and found that the spin-orbit interaction is large for certain crystallographic axes while it almost vanishes for other directions, reflecting its well-known anisotropy. This allows us to choose the strength of the spin-orbit interaction by the design of the device. Furthermore, we have measured the anisotropy of the spin flip rate depending on the direction of the applied in-plane magnetic field, which tunes the angle between the spin quantization axis and the spin-orbit field. The possibility to turn off the spin-orbit interaction enhances the spin coherence time in quantum dot devices, which is limited by the spin relaxation time. At high magnetic fields, we observe resonant spin-flip tunneling events, which can be used for coherent device operation.

We thank Peter Stano, Gian Salis, Patrick Altmann and Mattias Beck for stimulating discussions. We acknowledge QSIT via the SNF for providing the funding which enabled this work.

* andrea.hofmann@phys.ethz.ch

[1] R. Hanson, Rev. Mod. Phys. **79**, 1217 (2007).
[2] P. Scarlino, E. Kawakami, P. Stano, M. Shafiei, C. Reichl, W. Wegscheider, and L. Vandersypen, Phys. Rev. Lett. **113**, 256802 (2014).
[3] V. Maisi, A. Hofmann, M. Röösli, J. Basset, C. Reichl, W. Wegscheider, T. Ihn, and K. Ensslin, Phys. Rev. Lett. **116**, 136803 (2016).
[4] V. N. Golovach, A. Khaetskii, and D. Loss, Phys. Rev. Lett. **93**, 016601 (2004).
[5] P. Stano and J. Fabian, Phys. Rev. B **74**, 045320 (2006).
[6] A. V. Khaetskii and Y. V. Nazarov, Phys. Rev. B **64**, 125316 (2001).
[7] A. V. Khaetskii and Y. V. Nazarov, Phys. Rev. B **61**, 12639 (2000).
[8] D. V. Bulaev and D. Loss, Phys. Rev. B **71**, 205324 (2005).
[9] J. Danon, Phys. Rev. B **88**, 075306 (2013).
[10] J. Könemann, R. J. Haug, D. K. Maude, V. I. Fal'ko, and B. L. Altshuler, Phys. Rev. Lett. **94**, 226404 (2005).
[11] J. M. Nichol, S. P. Harvey, M. D. Shulman, A. Pal, V. Umansky, E. I. Rashba, B. I. Halperin, and A. Yacoby, Nature Communications **6**, 7682 (2015).
[12] C. W. J. Beenakker, Phys. Rev. B **44**, 1646 (1991).
[13] T. Ihn, *Semiconductor nanostructures: quantum states and electronic transport* (Oxford University Press, Oxford ; New York, 2010) oCLC: ocn430496978.
[14] L. M. K. Vandersypen, J. M. Elzerman, R. N. Schouten, L. H. W. v. Beveren, R. Hanson, and L. P. Kouwenhoven, Applied Physics Letters **85**, 4394 (2004).
[15] R. Schleser, E. Ruh, T. Ihn, K. Ensslin, D. C. Driscoll, and A. C. Gossard, Applied Physics Letters **85**, 2005 (2004).
[16] K. Ono, D. G. Austing, Y. Tokura, and S. Tarucha, Science **297**, 1313 (2002).
[17] A. C. Johnson, J. R. Petta, C. M. Marcus, M. P. Hanson, and A. C. Gossard, Phys. Rev. B **72**, 165308 (2005).
[18] T. Fujita, P. Stano, G. Allison, K. Morimoto, Y. Sato, M. Larsson, J.-H. Park, A. Ludwig, A. Wieck, A. Oiwa, and S. Tarucha, Phys. Rev. Lett. **117**, 206802 (2016).
[19] T. Fujita, K. Morimoto, H. Kiyama, G. Allison, M. Larsson, A. Ludwig, S. R. Valentin, A. D. Wieck, A. Oiwa, and S. Tarucha, arXiv:1504.03696 [cond-mat, physics:quant-ph] (2015), arXiv: 1504.03696.
[20] L. P. Kouwenhoven, D. G. Austing, and S. Tarucha, Rep. Prog. Phys. **64**, 701 (2001).
[21] F. H. L. Koppens, J. A. Folk, J. M. Elzerman, R. Hanson, L. H. W. v. Beveren, I. T. Vink, H. P. Tranitz, W. Wegscheider, L. P. Kouwenhoven, and L. M. K. Vandersypen, Science **309**, 1346 (2005).
[22] L. E. Reichl, *A modern course in statistical physics*, 4th ed. (Wiley-VCH Verlag GmbH & Co. KGaA, Weinheim, 2016) oCLC: 927845638.
[23] O. N. Jouravlev and Y. V. Nazarov, Phys. Rev. Lett. **96**, 176804 (2006).
[24] P. Stano and J. Fabian, Phys. Rev. B **72**, 155410 (2005).
[25] K. C. Nowack, F. H. L. Koppens, Y. V. Nazarov, and L. M. K. Vandersypen, Science **318**, 1430 (2007).
[26] A. Hofmann, V. Maisi, C. Gold, T. Krähenmann, C. Rössler, J. Basset, P. Märki, C. Reichl, W. Wegscheider, K. Ensslin, and T. Ihn, Phys. Rev. Lett. **117**, 206803 (2016).